RSC Advances

PAPER

View Article Online
View Journal | View Issue

Cite this: *RSC Adv.*, 2020, **10**, 5681

Additive manufacturing of SiBCN/Si_3N_4w composites from preceramic polymers by digital light processing†

Shan Li, *[a] Yubei Zhang,[a] Tong Zhao, [b] Weijian Han,[b] Wenyan Duan,[a] Li Wang,[a] Rui Dou*[a] and Gong Wang*[a]

Received 18th November 2019
Accepted 20th January 2020

DOI: 10.1039/c9ra09598e

rsc.li/rsc-advances

The application of advanced ceramic materials is limited by their brittleness and complicated manufacturing methods. Three-dimensional (3D) printing has emerged as a new method for the fabrication of complex-shaped ceramics. Herein, a type of printable slurry composed of SiBCN preceramic polymers and high-volume fractions of Si_3N_4 whiskers (up to 60 wt% of polymer) was prepared, and subsequently printed *via* digital light processing (DLP) technology. We successfully manufactured complex-structured ceramic composites and achieved high bending strength (~180 MPa). The linear shrinkage and mass loss of the ceramic material were both significantly reduced after the introduction of whiskers. The properties and structure of the printed parts pyrolyzed at different temperatures were compared, and the relationship between the microstructure and mechanical properties discussed.

1. Introduction

Ceramic composites are widely applied in high-tech fields such as in aerospace, new energy, electronics, and bio-engineering.[1–3] Nevertheless, ceramics are difficult to process due to their brittleness and poor melting. In addition, traditional ceramic-molding processes require complex methods that are time-consuming and expensive. Additive manufacturing, such as three-dimensional (3D) printing, is an emerging technology for the fabrication of complex ceramic components.[4–6] Stereolithography (SLA) and its derivatives (*i.e.*, digital light processing (DLP)) are a class of technologies that display much higher printing resolution compared with other 3D-printing methods.[7] Scholars have assessed the SLA 3D printing of various ceramic slurries,[8–11] such as ZrO_2,[8,12] Al_2O_3 (ref. 11 and 13) and hydroxyapatite.[10] The ceramic slurries were prepared by mixing ceramic powders with acrylate resins. However, some ceramic powders (*e.g.*, SiC, SiBCN, ZrC) exhibit a high refractive index, leading to high light refraction and absorption, which significantly reduces the light-penetration depth in the slurry material and disables the SLA printing process of the ceramic slurry.[14] Polymer-derived ceramic (PDC) routes provide another way of producing these materials. Hence, stereolithography of PDCs could be an effective method for fabricating these ceramics with high refractive indices.[5,15,16]

PDCs have been recognized widely as powerful tools for producing advanced ceramics. Their main advantage over conventional powder-synthetic procedures is the possibility of adopting a plastic-forming method to generate components with complex shapes that are subsequently transformed into the desired ceramic parts by heat treatment.[17,18] Intensive research has been conducted on the 3D printing of PDCs.[5,14–16,19,20] However, the liner shrinkage is relatively high (>25%), which may lead to collapse or some defects of the component.

The key problem is the control of shrinkage and structural integrity of the printed parts during the polymer-to-ceramic transformation. Introduction of inert fillers is an efficient way to reduce the shrinkage and porosity of the PDC[21] by diluting the percentage of polymer. Moreover, the use of fillers permits the manufacturing of ceramics with improved mechanical or functional properties.[21–23] Various fillers have been shown to be effective in strengthening PDCs, including carbon nanotubes, ceramic fibers, or graphene.[14,24,25]

SiBCN ceramics are a popular class of new ceramic materials with high thermal and phase stability.[26–29] Polyborosilazane (PBSZ), the precursor of SiBCN, is a liquid polymer with a high ceramic yield. In our previous work,[30] we modified PBSZ to render it photocurable (designated as "UV-PBSZ"). To decrease shrinkage of the printed parts during pyrolysis and improve the mechanical properties of the ceramic components, we assumed we introduced whiskers into UV-PBSZ. Whiskers of Si_3N_4 and SiC are fillers used commonly to improve the mechanical properties of the ceramic matrix,[31–33] whereas SiC whiskers

[a]*CAS Key Laboratory of Space Manufacturing Technology, Technology and Engineering Center for Space Utilization, Chinese Academy of Sciences, Beijing, 100094, P. R. China. E-mail: wanggong@csu.ac.cn; ruidou@csu.ac.cn*

[b]*Laboratory of Advanced Polymer Materials, Institute of Chemistry, Chinese Academy of Sciences, Beijing 100190, P. R. China*

† Electronic supplementary information (ESI) available. See DOI: 10.1039/c9ra09598e

affect DLP printing severely.[14] Herein, we manufactured Si_3N_4 whisker-filled SiBCN ceramic composite components with a complex shape and high resolution by DLP 3D-printing technology. Following pyrolysis, shrinkage of the component was much lower than that of the base preceramic polymer. A high bending strength of the printed ceramic composites was achieved, and the effects of the structure on the mechanical properties were discussed.

2. Experimental

2.1 Materials

The preceramic polymer used in this work was liquid PBSZ provided by the Laboratory of Advanced Polymer Materials, Institute of Chemistry, Chinese Academy of Sciences (Beijing, China). The multifunctional acrylate monomer, trimethylolpropane triacrylate (TMPTA), which exhibits high photopolymerization reactivity and high print precision, was purchased from Spaceworks (Beijing, China). A photoinitiator (IRGACURE 819) was used for printing experiments. Si_3N_4 whiskers were purchased from Forsman Scientific (Beijing, China). All chemicals were used as received.

2.2 Preparation of UV-PBSZ/Si_3N_4w

UV-PBSZ was prepared by mixing PBSZ and poly(2,2,6,6-tetramethylpiperidinyloxy-4-yl-methacrylate) (PTMA), as described in detail in our previous work.[30] The slurry was prepared by blending the UV-PBSZ and the Si_3N_4 whiskers in a weight ratio of 5 : 3. The mixture was stirred by ball-milling at 300 rpm for 4 h. A dispersant was used to make the slurry stable. Fig. s1† shows the viscosity curve of the slurry, including 60% (weight percentage of UV-PBSZ) Si_3N_4w loading at room temperature. The viscosity of the obtained slurry system was low (~30 mPa s), which is suitable for DLP 3D printing.

2.3 3D printing of the UV-PBSZ/Si_3N_4w system

3D printing of the slurry system was conducted on a DLP ceramic 3D printer produced by Spaceworks. The printer had a light source of wavelength 405 nm and DLP chip with 50 μm pixels. The exposure time and intensity were adjusted based on the photo-polymerization ability of the materials. During printing, the DLP printer projected patterned light that selectively exposed and hardened the material. Then, the cured material adhered to the printing platform. Following the printing of one layer, the platform ascended a distance of one-layer thickness above the vat. Subsequently, fresh photopolymer was re-coated on the bottom of the vat, and UV light cured the subsequent layer. This process was repeated for each designed layer until the 3D objects were printed completely.

During printing, the photo-polymerization reaction was triggered; the crosslinking of the photosensitive groups in UV-PBSZ generated a polymer network that acted as a framework entrapping the Si_3N_4 whiskers. Introduction of the fillers might affect the photocuring process. Fig. 1 shows the curing depth of the slurry containing different amount of Si_3N_4 whiskers: the curing depth decreased significantly after introduction of the Si_3N_4 whiskers. With an increase in Si_3N_4w contents, the curing depth decreased further; when the Si_3N_4 loading was 60%, the curing depth was only 90 μm under a relatively high UV dose (528 mW S cm^{-2}). With the increase of the UV dose, the curing depth of the base UV-PBSZ increased sharply, whereas that of the slurry increased slightly, suggesting that the whiskers would severely affect UV curing even under a higher UV dose. When the Si_3N_4 loading increased further, it was very hard to print.

For maximum reduction in the shrinkage of the 3D printing of PDCs, we used a printable slurry with maximum loading (60%). The slurry was fabricated with a layer thickness of 50 μm and exposure dose of 528 mW S cm^{-2}. The material system remained printable even at high loading of Si_3N_4 whiskers (60 wt%), which was attributed to the high UV sensitivity of the preceramic polymer and the adjustable wide-range exposure dose of the printer.

2.4 Pyrolysis of 3D-printed parts

The polymer-to-ceramic transformation was done in an alumina tube furnace under a nitrogen atmosphere. The printed green bodies were first heated at a constant rate of 0.5 °C min^{-1} from room temperature to 600 °C, then heated up to 900 °C at a heating rate of 1 °C min^{-1} and held at 900 °C for 1 h; finally, they were cooled at 3 °C min^{-1} to room temperature. To achieve different ceramic structures, the samples were sintered at 900 °C, 1200 °C, or 1400 °C for 1 h at the same heating rate (1 °C min^{-1}) and cooling rate (3 °C min^{-1}), and the corresponding samples were designated "composite900", "composite1200" and "composite1400", respectively.

2.5 Characterization

Thermogravimetric analysis (TGA) was carried out with a STA409PC (Netzsch, Selb, Germany) system at a heating rate of 10 °C min^{-1} in a nitrogen atmosphere. The microstructure of the printed samples was observed on a scanning electron microscope (S-4800; Hitachi, Tokyo, Japan) at an accelerating voltage of 10 kV. The flexure strength of the sintered samples

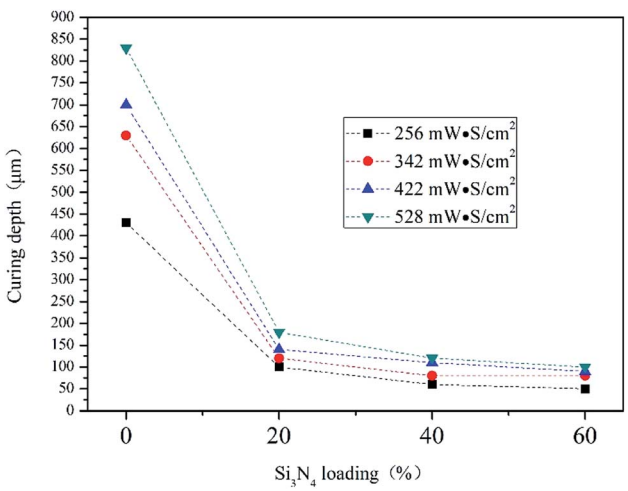

Fig. 1 Curing depth of slurries with different Si_3N_4 loadings.

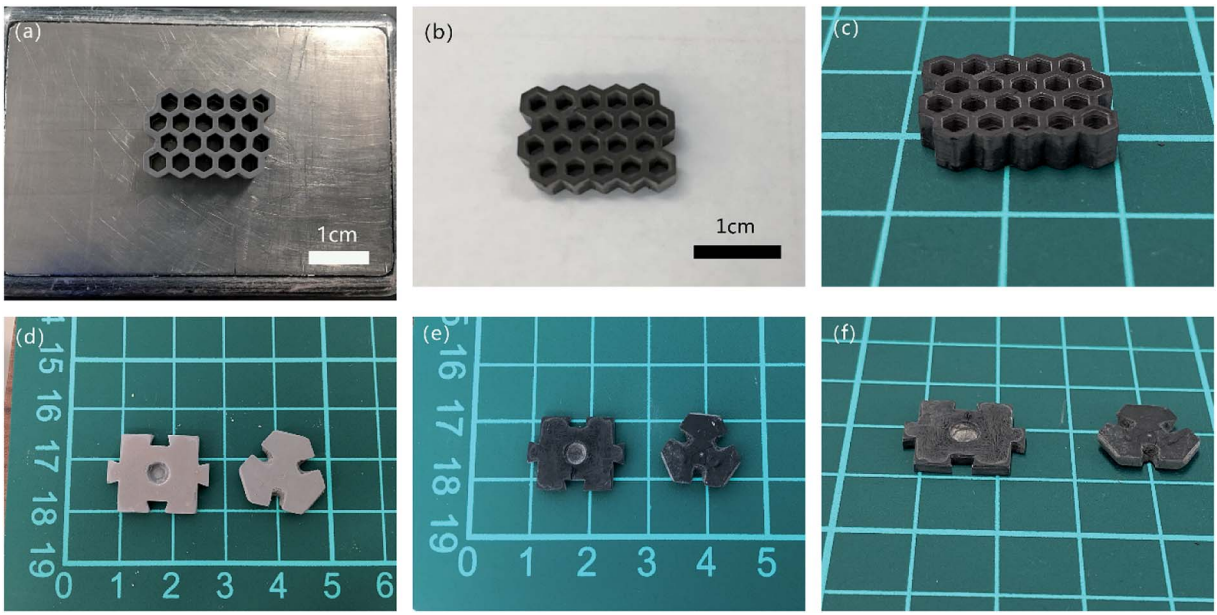

Fig. 2 Optical images of (a and d) printed parts and (b, c, e and f) the corresponding sintered parts: (b and e) top view and (c and f) orthogonal image.

was investigated using a computer-controlled testing machine (5569; Instron, Norwood, MA, USA) with a span of 9 mm and crosshead speed of 0.5 mm min^{-1} at room temperature. The testing standards for the flexure strength were according to the three-point bending test. Five specimens (2.4 × 4.0 × 18 mm) were tested to obtain the mean value. Nanoindentation tests were undertaken on a Triboindenter (Hysitron, Minneapolis, MN, USA). Chunks of sintered samples were mounted and then indented using a sharp diamond indenter with an indentation load of 100 mN. Five indentations were taken and mean values were calculated. X-ray diffraction (XRD) spectroscopy was done in reflection mode on a powder X-ray diffractometer (D/max 2500; Cu–Kα radiation λ = 1.4518 Å; Rigaku, Tokyo, Japan).

3. Results and discussion

The schematic chemical structure of polyborosilazane (PBSZ) and trimethylolpropane triacrylate (TMPTA) are shown in Fig. s2.† The main chain of PBSN was composed of Si–N and B–N bonds. The vinyl groups on PBSZ could contribute to UV curing. TMPTA has three functional acrylate groups, which exhibit very high photocuring activity. During printing, the vinyl and acrylate groups were crosslinked through polymerization.[15]

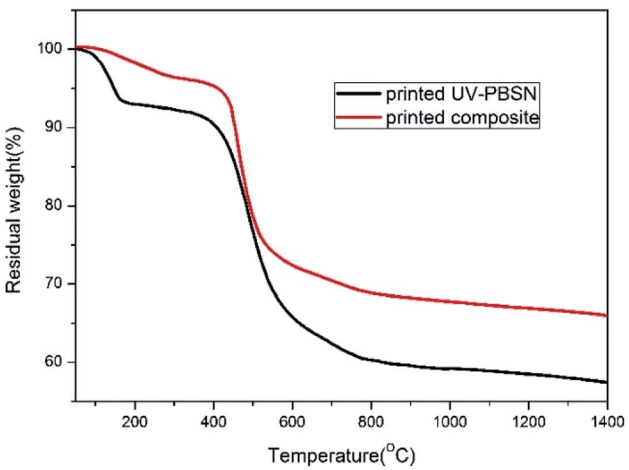

Fig. 3 TGA curves of the printed UV-PBSZ and printed composite slurry.

The scanning electron microscopy (SEM) image (Fig. s3†) showed that the whiskers had a diameter of approximately 2–4 μm and length of 5–20 μm, thereby showing a wide size distribution. The XRD spectrum (Fig. s4†) revealed that the whiskers

Table 1 Typical parameters of the samples sintered at different temperatures

Material	*x*/*y*	*z*	Residual weight (%)	Density (g cm^{-3})
SiBCN1200 (ref. 30)	28.0 ± 0.1	30.9 ± 0.2	58.1 ± 0.1	1.85 ± 0.05
Composite900	18.1 ± 0.1	21.3 ± 0.1	74.8 ± 0.1	2.15 ± 0.05
Composite1200	18.5 ± 0.1	22.5 ± 0.1	72.2 ± 0.1	2.10 ± 0.05
Composite1400	18.7 ± 0.1	22.6 ± 0.1	70.4 ± 0.1	2.15 ± 0.05

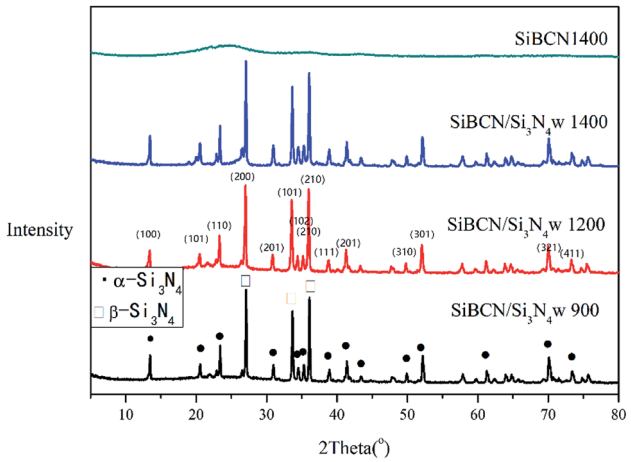

Fig. 4 XRD spectra of samples sintered at different temperatures.

were composed of α-Si_3N_4 and β-Si_3N_4. The reflections located at $2\theta = 13°$, 21°, 34°, 36°, 41°, 51°, 71° and 73° were ascribed to α-Si_3N_4, and the signals at $2\theta = 23°$, 27°, 33° and 37° belonged to β-Si_3N_4.

Ceramic composite components were printed and sintered (Fig. 2). The printed green body had fine and complicated features with a smooth surface, suggesting a high resolution of the DLP-printing technology. After sintering, the shape of the components was well preserved without visible deformation or macro-cracks due to the low liner shrinkage of the component. Obtaining solid block structures through PDC routes are difficult due to the cracking problem of PDCs during pyrolysis. Furthermore, investigation of mechanical properties of PDCs has been hindered due to limitations in fabrication of suitable bulk test specimens.

The shrinkage and residual weight of the composites sintered at different temperatures are provided in Table 1. The linear shrinkage of pure UV-PBSZ was ~30%, whereas that of the composite was ~20%, suggesting that introduction of Si_3N_4 whiskers could significantly reduce the linear shrinkage of the printed parts during sintering, and maintain the stability of the structures. With an increase in pyrolysis temperature, the shrinkage of all three axes increased slightly. For example, the linear shrinkage of the *x*/*y* axes was 18.1%, 18.5% and 18.7% for samples pyrolyzed at 900 °C, 1200 °C and 1400 °C, respectively. The shrinkage in the three axes was different, with the *x*/*y* axes having lower and the *z* axis having the larger shrinkage (likely due to the *z* axis being the printing direction and the interlayer lamination becoming denser after sintering). Compared with the base resin UV-PBSZ, the residual weight of the composite

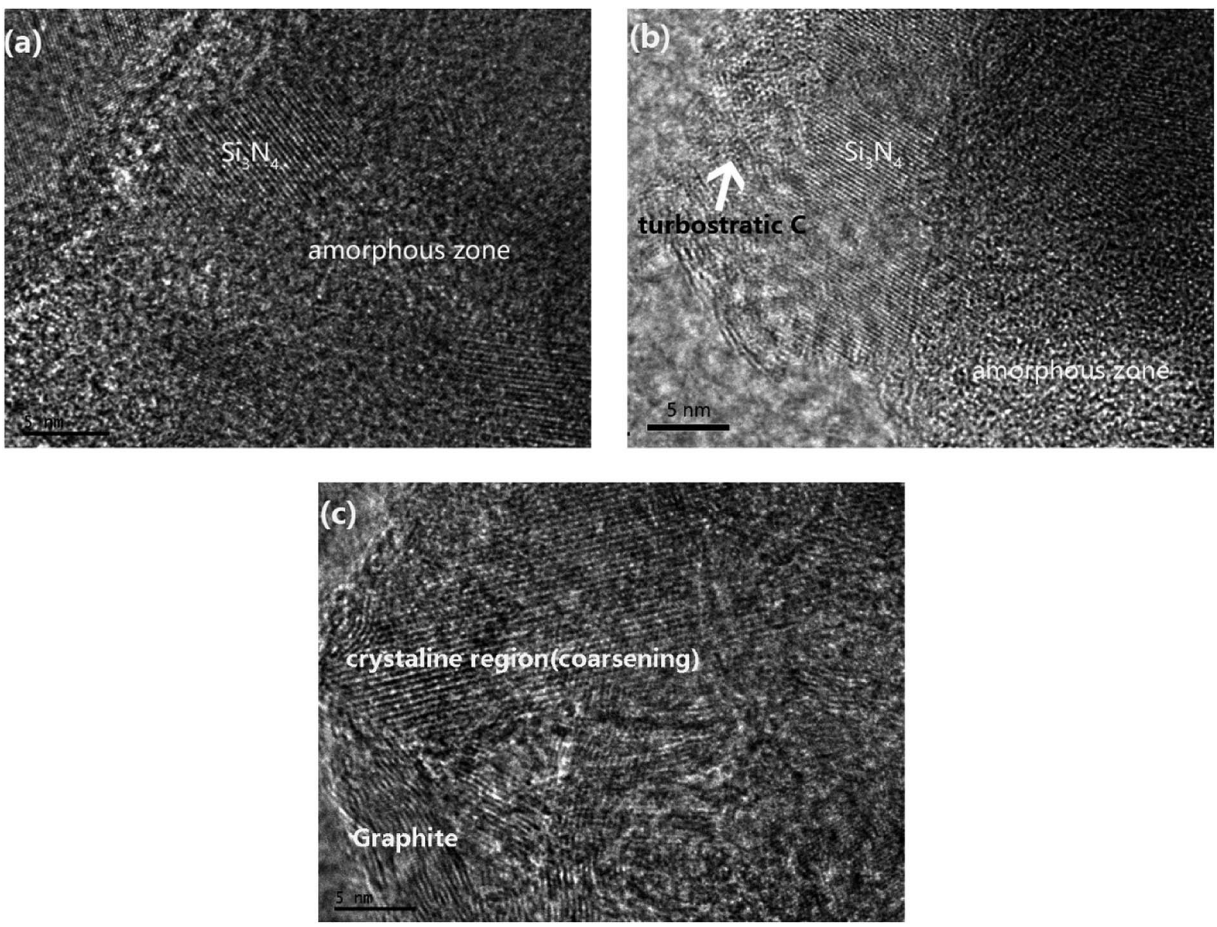

Fig. 5 TEM images of composites sintered at (a) 900 °C, (b) 1200 °C and (c) 1400 °C.

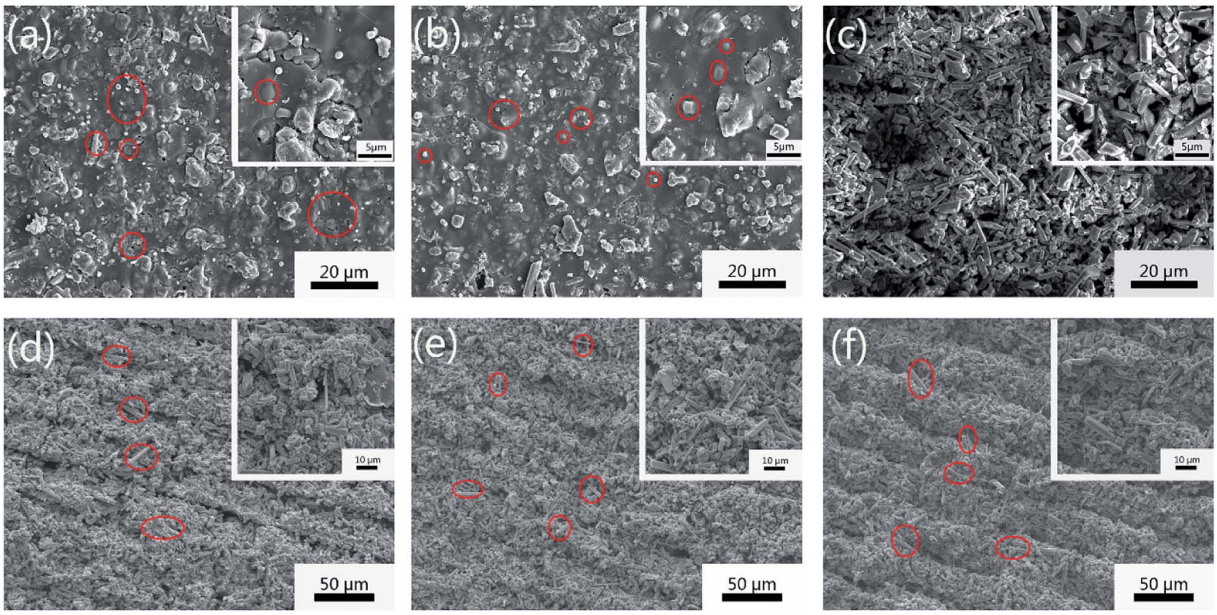

Fig. 6 (a–c) Surface and (d–f) cross-sectional SEM images of the sintered parts at (a and d) 900 °C, (b and e) 1200 °C, and (c and f) 1400 °C.

also improved significantly, from 58.1% for UV-PBSZ to 72.2% for composite1200. With an increase in sintering temperature, the residual weight also decreased slightly, from 74.8% for composite900 to 70.4% for composite1400. The density of the composite was measured according to the Archimedes principle. The density of the base resin was ~1.85 g cm^{-3}, whereas the density of the composite was ~2.1 g cm^{-3}. The slight increase in the density may have been caused by the high content of Si_3N_4 whiskers in the composite. The density of the composite sintered at different temperatures was essentially identical.

The weight changes of the printed UV-PBSZ and composites during high-temperature sintering were assessed by TGA (Fig. 3). The weight loss of both systems occurred mainly in two steps. The first step was between room temperature to 300 °C, and the second step from 400 to 700 °C. The temperature at which maximum decomposition occurred was ~450 °C, at which point the organic moiety in the material system could be decomposed. Above 800 °C, the weight change was milder, indicating that the polymer-to-ceramic conversion was almost complete. The thermal stability of the printed composite was higher than that of printed UV-PBSZ due to the dilution effect of the filled inert whiskers in the composite. The residual weight of the base resin and composite at 1000 °C was ~58% and ~68%, respectively, which suggested a much higher residual weight in the composite.

XRD spectroscopy was conducted to investigate the crystallization behavior of the ceramic material sintered at different temperatures (Fig. 4). After pyrolysis at 900 °C, the main composition was Si_3N_4 with peaks at $2\theta = 13°$, 23°, 27°, 33°, 37°, 41°, 51°, 71° and 73°. With an increase in the pyrolysis temperature, the signals of graphitic carbon at around $2\theta = 26°$ became more obvious. The reflections of β-SiC, which were located at $2\theta = 36°$, 60° and 72°, were covered by the signals of Si_3N_4, and distinguishing them was difficult. Compared with the structure of the base resin (SiBCN 1400) that remained amorphous until 1400 °C, the crystallization resistance of the composite decreased due to the high amounts of Si_3N_4 whiskers in the material system.

Table 2 Mechanical properties of PDC specimens processed by different methods

Material	Method	Flexural strength (MPa)	Hardness (GPa)	Modulus (GPa)
Cf/SiOC[36]	PIP	253.3		33.3
SiC[37]	PIP	85 ± 5	30	218
SiCN[35]	Cold isostatic pressing	118	6.1	105
SiCN[4]	DLP printing	57.3 ± 8.7		
SiBCN1200 (ref. 30)	DLP printing		7.8 ± 0.3	54.7 ± 0.3
Composite900	DLP printing	**128 ± 15**		**28.4 ± 0.2**
Composite1200	DLP printing	**183 ± 13**	**3.4 ± 0.2**	**54.1 ± 0.3**
Composite1400	DLP printing	**68 ± 18**		

Transmission electron microscopy (TEM) was used to investigate further the microstructure of the composite sintered at different temperatures (Fig. 5). For composite900, TEM showed Si_3N_4 crystallites and the amorphous matrix. After sintering at 1200 °C, turbostratic carbon features were formed along the Si_3N_4 crystallites, but major changes in the overall microstructure of the sample were not observed, and these data were consistent with the results of XRD spectroscopy. At a higher temperature (1400 °C), coarsening of the crystallites was observed, and the turbostratic carbon transformed into ordered graphite of thickness 4–10 nm, which was also observed in the XRD spectrum.

Si_3N_4 crystallites may promote matrix crystallization. Pure PDCs can retain an amorphous structure until a much higher temperature (1500 °C) through a diffusion barrier (turbostratic BNCx) limiting the size of the crystal domains. After

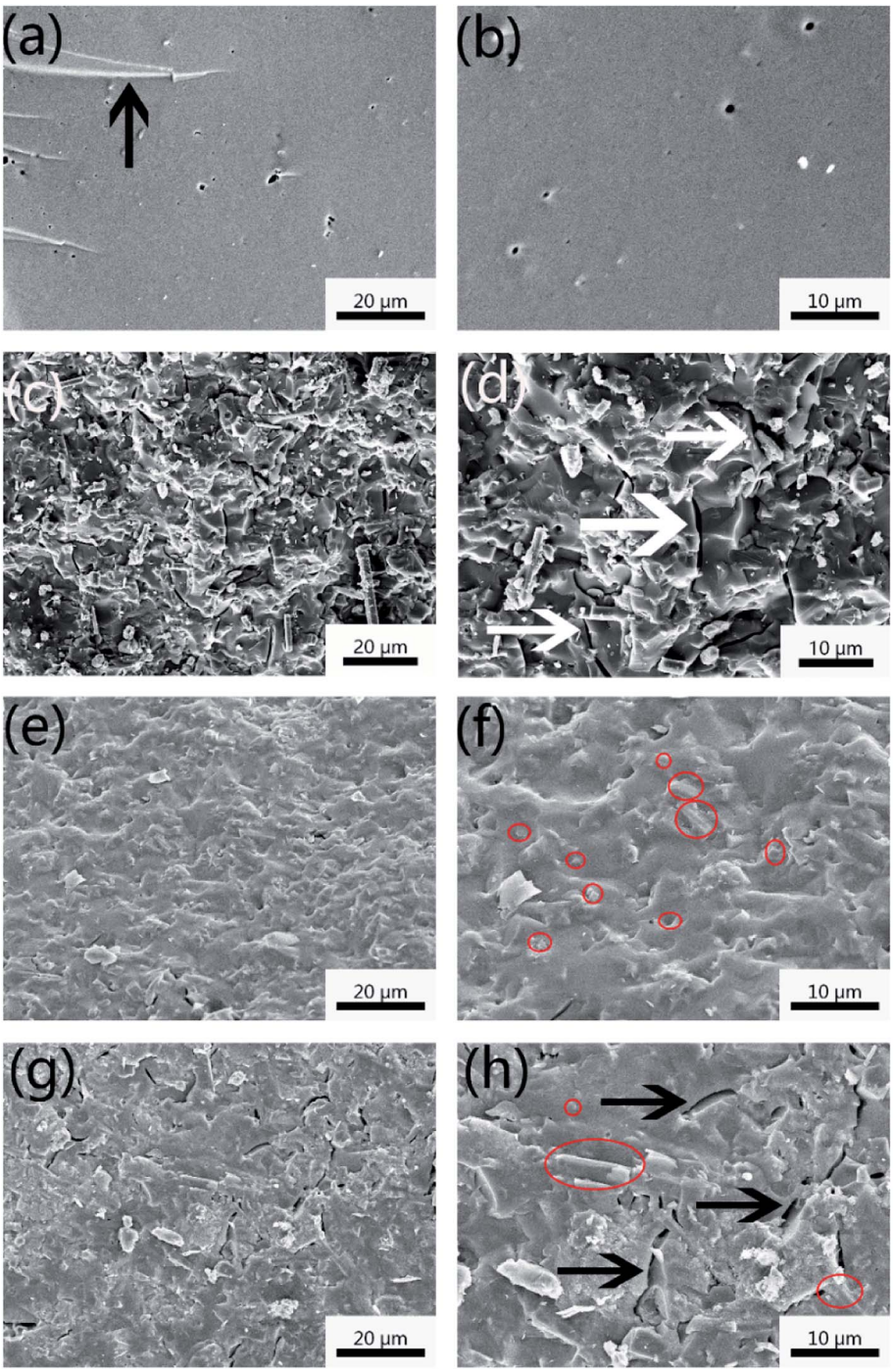

Fig. 7 Fracture surface of the sintered parts (a and b) base SiBCN at 1400 °C, (c and d) composite900, (e and f) composite1200 and (g and h) composite1400; (b, d, f and h) at high magnifications (a, c, e and g).

introduction of Si_3N_4 crystallites, the amorphous interconnecting network of the matrix shows local disruption, and then initiation of crystallization begins, resulting in the loss of stability at high temperatures.

The microstructure of samples sintered at different temperatures was investigated by SEM (Fig. 6). The white dots and particles (marked by red circles) on the surface of composite900 (Fig. 6a) were determined to be Si_3N_4 whiskers. Composite1200 (Fig. 6b) showed a similar morphology to that of comosite900. At a higher temperature (1400 °C), the surface of the sample became rough, and more whiskers were exposed on the surface (Fig. 6c). During pyrolysis, the preceramic polymer pyrolyzed, resulting in linear shrinkage of the matrix parts, whereas the Si_3N_4 whiskers retained their dimensions and protruded from the surface. After sintering at 1400 °C, further decomposition of the PDC matrix led to many more exposed whiskers without the matrix binder.

The cross-sectional images (Fig. 6d–f) of the composites pyrolyzed at different temperatures showed a similar morphology. There was no interlayer gap between the printing layers, which suggested good interlayer bonding. Undulations were found on the cross-sectional surface of the printed part, which was caused by the layer-by-layer printing process. In the higher-magnification images (upper-right corner of the figure), whiskers were dispersed uniformly within the matrix.

The mechanical properties of the ceramic composites were evaluated (Table 2). The bending strength of the composite reached 183 MPa upon sintering at 1200 °C. For the base SiBCN ceramic, the bending strength was too low to be measured for the samples sintered at all temperatures. Therefore, the Si_3N_4 whiskers helped to improve the mechanical properties of the PDC. The flexure strength of composite1200 (183 MPa) was higher than the reported values (57.3 MPa) of PDCs fabricated by DLP-printing technology, and is also at the same level with PDCs processed through other methods.[34–37] A nanoindentation test was undertaken to calculate the hardness and modulus. Composite1200 showed higher hardness (3.4 GPa) and modulus (54.1 GPa) than composite900 and composite1400. The monolithic SiBCN ceramic showed the highest hardness of 7.8 GPa and modulus of 54.7 GPa. The mechanism of the different mechanical properties was analyzed by a microstructure study.

The fracture surface of the tested samples sintered at different temperatures was investigated by SEM (Fig. 7). The fracture surface of the printed monolithic SiBCN ceramic material was smooth, suggesting that the material was brittle. Conversely, the fracture surface of the composite was uneven, indicating a ductility fracture. Composite900 showed micro-cracks in the fracture surface due to the brittle features of the incomplete ceramic transformation of the precursor matrix (arrows in Fig. 7d). For composite1200 (Fig. 7f), micro-cracks were not observed, and the whiskers merged within the ceramic matrix and were closely connected. Subsequent sintering at 1400 °C let to formation of many cracks in the fracture surface (Fig. 7h), and the reason is explicable.

When the pyrolysis temperature was low (900 °C), the preceramic polymer did not convert to a ceramic completely, exhibiting a low strength, and the matrix tended to form cracks during mechanical testing. For composite1400, the microstructure of the PDC matrix began to coarsen, and the crystals became larger (Fig. 5c), resulting in the loss of thermal stability. The PDC matrix decomposed slightly (Fig. 6c), with whiskers being exposed on the surface. Cracks were formed due to decomposition of the PDC matrix (Fig. 7h), which acted as defects in the sample, leading to a sharp decrease in mechanical properties. In composite1200, the perfect fracture surface without microcracks and better boundary connection between whiskers and the ceramic matrix than that in other composites contributed to the excellent mechanical properties.[31] Whiskers can act as the reinforced phase in the composite, thereby enhancing the strength of the ceramic material.

4. Conclusions

SiBCN/Si_3N_4w composites were fabricated through DLP 3D-printing technology. A printable preceramic slurry containing a preceramic polymer (polyborosilazane) and high amount of Si_3N_4 whiskers (60 wt% of the polymer) was prepared and printed into complicated components. The shrinkage was only 18% in the *x*/*y* direction during pyrolysis, which is very low among the 3D printing of PDCs. The bending strength was improved at 183 MPa (higher than the reported data of the DLP printing of PDCs) for the printed composite sintered at 1200 °C, which was due to the strength effect of the high amount of whiskers.

DLP 3D-printing technology has shown great potential in shape-forming of ceramic composites with complex structures. SiBCN/Si_3N_4w composites with specially designed complex structures and improved mechanical properties can be fabricated more efficiently and readily, which can act as a thermal-barrier layer in hypersonic aircraft wings. Our method proposed is also applicable for the manufacture of other ceramic composites.

Funding

The authors gratefully acknowledge the financial support of the Technology and Engineering Center for Space Utilization (CSU-QZKT-201807), Natural Science Foundation of Beijing (2204102 and 3194063) and Natural Science Foundation of China (51802319).

Conflicts of interest

There are no conflicts to declare.

Acknowledgements

The authors would like to thank Tong Zhao for the supply of the preceramic polymer, Xin Li for the adjusting and testing of the printer, and Xiaodong Liu for the CAD design of the models. The authors gratefully acknowledge the financial support of the Technology and Engineering Center for Space Utilization (No. CSU-QZKT-201807) and the Natural Science Foundation of

Beijing (Grant: 2204102 and 3194063) and Natural Science Foundation of China (Grant: 51802319).

References

1 R. He, W. Liu, Z. Wu, *et al.*, Fabrication of complex-shaped zirconia ceramic parts *via* a DLP-stereolithography-based 3d printing method, *Ceram. Int.*, 2018, **44**, 3412–3416.

2 Z. Li, B. Peng, T. Zhang, *et al.*, Improving sealing performance of borosilicate glass-ceramics for solid oxide fuel cell applications: effect of AlN, *J. Eur. Ceram. Soc.*, 2019, **39**, 4194–4201.

3 C. Paredes, F. J. Martínez-Vázquez, A. Pajares and P. Miranda, Development by robocasting and mechanical characterization of hybrid HA/PCL coaxial scaffolds for biomedical applications, *J. Eur. Ceram. Soc.*, 2019, **39**, 4375–4383.

4 C.-J. Bae and J. W. Halloran, Integrally cored ceramic mold fabricated by ceramic stereolithography, *Int. J. Appl. Ceram. Technol.*, 2011, **8**, 1255–1262.

5 Z. C. Eckel, C. Zhou, J. H. Martin, A. J. Jacobsen, W. B. Carter and T. A. Schaedler, Additive manufacturing of polymer-derived ceramics, *Science*, 2016, **351**, 58–62.

6 M. Lasgorceix, E. Champion and T. Chartier, Shaping by microstereolithography and sintering of macro–micro-porous silicon substituted hydroxyapatite, *J. Eur. Ceram. Soc.*, 2016, **36**, 1091–1101.

7 K. Li and Z. Zhao, The effect of the surfactants on the formulation of UV-curable SLA alumina suspension, *Ceram. Int.*, 2017, **43**, 4761–4767.

8 Q. Lian, W. Sui, X. Wu, F. Yang and S. Yang, Additive manufacturing of ZrO_2 ceramic dental bridges by stereolithography, *Rapid Prototyp. J.*, 2018, **24**, 114–119.

9 H. Wu, W. Liu, R. He, *et al.*, Fabrication of dense zirconia-toughened alumina ceramics through a stereolithography-based additive manufacturing, *Ceram. Int.*, 2017, **43**, 968–972.

10 Y. Zeng, Y. Yan, H. Yan, *et al.*, 3D printing of hydroxyapatite scaffolds with good mechanical and biocompatible properties by digital light processing, *J. Mater. Sci.*, 2018, **53**, 6291–6301.

11 S. Zhang, N. Sha and Z. Zhao, Surface modification of α-Al_2O_3 with dicarboxylic acids for the preparation of UV-curable ceramic suspensions, *J. Eur. Ceram. Soc.*, 2017, **37**, 1607–1616.

12 H. Shao, D. Zhao, T. Lin, J. He and J. Wu, 3d gel-printing of zirconia ceramic parts, *Ceram. Int.*, 2017, **43**, 13938–13942.

13 D. An, H. Li, Z. Xie, *et al.*, Additive manufacturing and characterization of complex Al_2O_3 parts based on a novel stereolithography method, *Int. J. Appl. Ceram. Technol.*, 2017, **14**, 836–844.

14 S. A. Brinckmann, N. Patra, J. Yao, T. H. Ware, C. P. Frick and R. S. Fertig, Stereolithography of SiOC polymer-derived ceramics filled with SiC micronwhiskers, *Adv. Eng. Mater.*, 2018, **20**, 1800593.

15 Y. de Hazan and D. Penner, SiC and SiOC ceramic articles produced by stereolithography of acrylate modified polycarbosilane systems, *J. Eur. Ceram. Soc.*, 2017, **37**, 5205–5212.

16 J. Schmidt and P. Colombo, Digital light processing of ceramic components from polysiloxanes, *J. Eur. Ceram. Soc.*, 2018, **38**, 57–66.

17 P. Colombo, J. Schmidt, G. Franchin, A. Zocca and J. Gunster, Additive manufacturing techniques for fabricating complex ceramic components from preceramic polymers, *Am. Ceram. Soc. Bull.*, 2017, **96**, 16–23.

18 E. Zanchetta, M. Cattaldo, G. Franchin, *et al.*, Stereolithography of SiOC ceramic microcomponents, *Adv. Mater.*, 2016, **28**, 370–376.

19 P. Jana, O. Santoliquido, A. Ortona, P. Colombo and G. D. Sorarù, Polymer-derived SiCN cellular structures from replica of 3d printed lattices, *J. Am. Ceram. Soc.*, 2018, **101**, 2732–2738.

20 M. Wang, C. Xie, R. He, *et al.*, Polymer-derived silicon nitride ceramics by digital light processing based additive manufacturing, *J. Am. Ceram. Soc.*, 2019, **102**, 5117–5126.

21 E. Bernardo, L. Fiocco, G. Parcianello, E. Storti and P. Colombo, Advanced ceramics from preceramic polymers modified at the nano-scale: a review, *Materials*, 2014, **7**, 1927–1956.

22 E. Bernardo, P. Colombo and S. Hampshire, Advanced ceramics from a preceramic polymer and nano-fillers, *J. Eur. Ceram. Soc.*, 2009, **29**, 843–849.

23 P. Colombo, E. Bernardo and G. Parcianello, Multifunctional advanced ceramics from preceramic polymers and nano-sized active fillers, *J. Eur. Ceram. Soc.*, 2013, **33**, 453–469.

24 Y. Azizian-Kalandaragh, A. S. Namini, Z. Ahmadi and M. Shahedi Asl, Reinforcing effects of SiC whiskers and carbon nanoparticles in spark plasma sintered ZrB_2 matrix composites, *Ceram. Int.*, 2018, **44**, 19932–19938.

25 Y. Luo, S.-l. Zheng, S.-h. Ma, C.-l. Liu and X.-h. Wang, Mullite-bonded SiC-whisker-reinforced SiC matrix composites: preparation, characterization, and toughening mechanisms, *J. Eur. Ceram. Soc.*, 2018, **38**, 5282–5293.

26 J. Li, M. Zhao, Y. Liu, *et al.*, Microstructure and dielectric properties of LPCVD/CVI-SiBCN ceramics annealed at different temperatures, *Materials*, 2017, **10**, 655–666.

27 S. Li, Y. Luo, L. Wang and C. Xu, Polyborosilazane preceramic as matrix resin of high temperature adhesive for graphite bonding, *Int. J. Appl. Ceram. Technol.*, 2017, **14**, 999–1005.

28 C. Zhang, K. Han, Y. Liu, *et al.*, A novel high yield polyborosilazane precursor for SiBNC ceramic fibers, *Ceram. Int.*, 2017, **43**, 10576–10580.

29 H. Zhao, L. Chen, X. Luan, X. Zhang, J. Yun and T. Xu, Synthesis, pyrolysis of a novel liquid SiBCN ceramic precursor and its application in ceramic matrix composites, *J. Eur. Ceram. Soc.*, 2017, **37**, 1321–1329.

30 S. Li, W. Duan, T. Zhao, *et al.*, The fabrication of SiBCN ceramic components from preceramic polymers by digital light processing (DLP) 3d printing technology, *J. Eur. Ceram. Soc.*, 2018, **38**, 4597–4603.

31 C.-Y. Chu, J. P. Singh and J. L. Routbort, High-temperature failure mechanisms of hot-pressed Si_3N_4 and Si_3N_4/Si_3N_4-

whisker-reinforced composites, *J. Am. Ceram. Soc.*, 1993, **76**, 1349–1353.

32 J. Homeny and L. J. Neergaard, Mechanical properties of beta-Si_3N_4-whisker/Si_3N_4-matrix composites, *J. Am. Ceram. Soc.*, 1990, **73**, 3493–3496.

33 W. J. Tseng and P. D. Funkenbusch, Microstructure and densification of pressureless-sintered Al_2O_3/Si_3N_4-whisker composites, *J. Am. Ceram. Soc.*, 1992, **75**, 1171–1175.

34 P. Colombo, G. Mera, R. Riedel and G. D. Sorarù, Polymer-derived ceramics: 40 years of research and innovation in advanced ceramics, *J. Am. Ceram. Soc.*, 2010, **93**, 1805–1837.

35 T. Nishimura, R. Haug, J. Bill, G. Thurn and F. Aldinger, Mechanical and thermal properties of Si–C–N material from polyvinylsilazane, *J. Mater. Sci.*, 1998, **33**, 5237–5241.

36 Q. Yuan, Z.-F. Chai, Z.-R. Huang and Q. Huang, A new precursor of liquid and curable polysiloxane for highly cost-efficient SiOC-based composites, *Ceram. Int.*, 2019, **45**, 7044–7048.

37 S. C. Zunjarrao, A. Rahman, R. P. Singh and R. Reidel, Characterization of the evolution and properties of silicon carbide derived from a preceramic polymer precursor, *J. Am. Ceram. Soc.*, 2013, **96**, 1869–1876.